International Journal of Solids and Structures 117 (2017) 137–142

Contents lists available at ScienceDirect

International Journal of Solids and Structures

journal homepage: www.elsevier.com/locate/ijsolstr

Collapse of liquid-overfilled strain-isolation substrates in wearable electronics

Xiufeng Wang[a,b], Yinji Ma[a,c,*], Yeguang Xue[a], Haiwen Luan[a], Matt Pharr[d], Xue Feng[c], John A. Rogers[e], Yonggang Huang[a,*]

[a] Department of Civil and Environmental Engineering, Mechanical Engineering, and Materials Science and Engineering, Northwestern University, Evanston, IL 60208, USA
[b] School of Materials Science and Engineering, Xiangtan University, Hunan, 411105, China
[c] Department of Engineering Mechanics, Center for Mechanics and Materials, Tsinghua University, Beijing, 100084, China
[d] Department of Mechanical Engineering, Texas A&M University, College Station, TX 77843, USA
[e] Department of Materials Science and Engineering, Chemistry, Mechanical Science and Engineering, Electrical and Computer Engineering Beckman Institute for Advanced Science and Technology, and Frederick Seitz Materials Research Laboratory, University of Illinois at Urbana-Champaign, Urbana, IL 61801, USA

ARTICLE INFO

Article history:
Received 18 December 2016
Revised 17 March 2017
Available online 30 March 2017

Keywords:
Wearable electronics
Strain isolation
Roof collapse
Air-filled
Liquid-filled
Liquid-overfilled cavities

ABSTRACT

Liquid that resides in a soft elastomer embedded between wearable electronics and biological tissue provides a strain-isolation effect, which enhances the wearability of the electronics. One potential drawback of this design is vulnerability to structural instability, e.g., roof collapse may lead to partial closure of the liquid-filled cavities. This issue is addressed here by overfilling liquid in the cavities to prevent roof collapse. Axisymmetric models of the roof collapse are developed to establish the scaling laws for liquid-overfilled cavities, as well as for air- and liquid-filled ones. It is established that the liquid-overfilled cavities are most effective to prevent roof collapse as compared to air- and liquid-filled ones.

1. Introduction

Soft (Cheng et al., 2011; Kim et al., 2009; Wu et al., 2010) or stiff substrates (Robinson et al., 2014; Romeo et al., 2013), embedded between wearable electronics (Chen et al., 2016; Chortos et al., 2016; Webb et al., 2015; Xu and Zhu, 2012) and biological tissues, can shield the electronics from strains induced by the biological tissue, i.e., they can provide "strain isolation". The soft substrates also shield the biological tissues from sensing the existence of the wearable electronics (Koh et al., 2016; Lee et al., 2015). A new design (Ma et al., 2017) introduces cavities in the substrate in order to enhance the strain-isolation effect. One potential drawback of this design is that the cavities may close due to adhesion (the so called "roof collapse" (De Boer and Michalske, 1999; Huang et al., 2005; Mastrangelo and Hsu, 1993)), which eliminates the desired strain-isolation effects. Ma et al. (2017) proposed injecting liquid into the cavities to prevent roof collapse, and they also developed two-dimensional models for air-filled and liquid-filled cavities; however, a 2D model may significantly overestimate roof collapse (Xue et al., 2017).

A more effective method to overcome roof collapse is proposed in this paper by overfilling liquid in the cavities. For circular cavities implemented in the experiments, axisymmetric models are more accurate than 2D ones, and are thus developed for liquid-overfilled cavities, as well as air- and liquid-filled ones. A scaling law is developed to give the critical work of adhesion, below which roof collapse will not occur. This critical work of adhesion depends strongly on the amount of liquid overfill.

2. Analytic model of collapse

Fig. 1 shows the schematic illustrations of roof collapse of circular air-filled (Fig. 1a and b), liquid-filled (Fig. 1c and d) and liquid-overfilled (Fig. 1e and f) cavities (radius R and height h) in the substrate, with the collapse radius αR to be determined. The layers above and below the cavity are called the top layer and bottom layer of the substrate, which is sandwiched between the circular electronic device (radius κR, thickness t_1, modulus E_1, and Poisson's ratio ν_1) and the biological tissue. Roof collapse of the cavity occurs mainly due to the deformation of the top layer (thickness t_2, modulus E_2, and Poisson's ratio $\nu_2 = 0.5$ for most elastomers)

* Corresponding authors.
E-mail addresses: mayinji@gmail.com (Y. Ma), y-huang@northwestern.edu (Y. Huang).

http://dx.doi.org/10.1016/j.ijsolstr.2017.03.031
0020-7683/

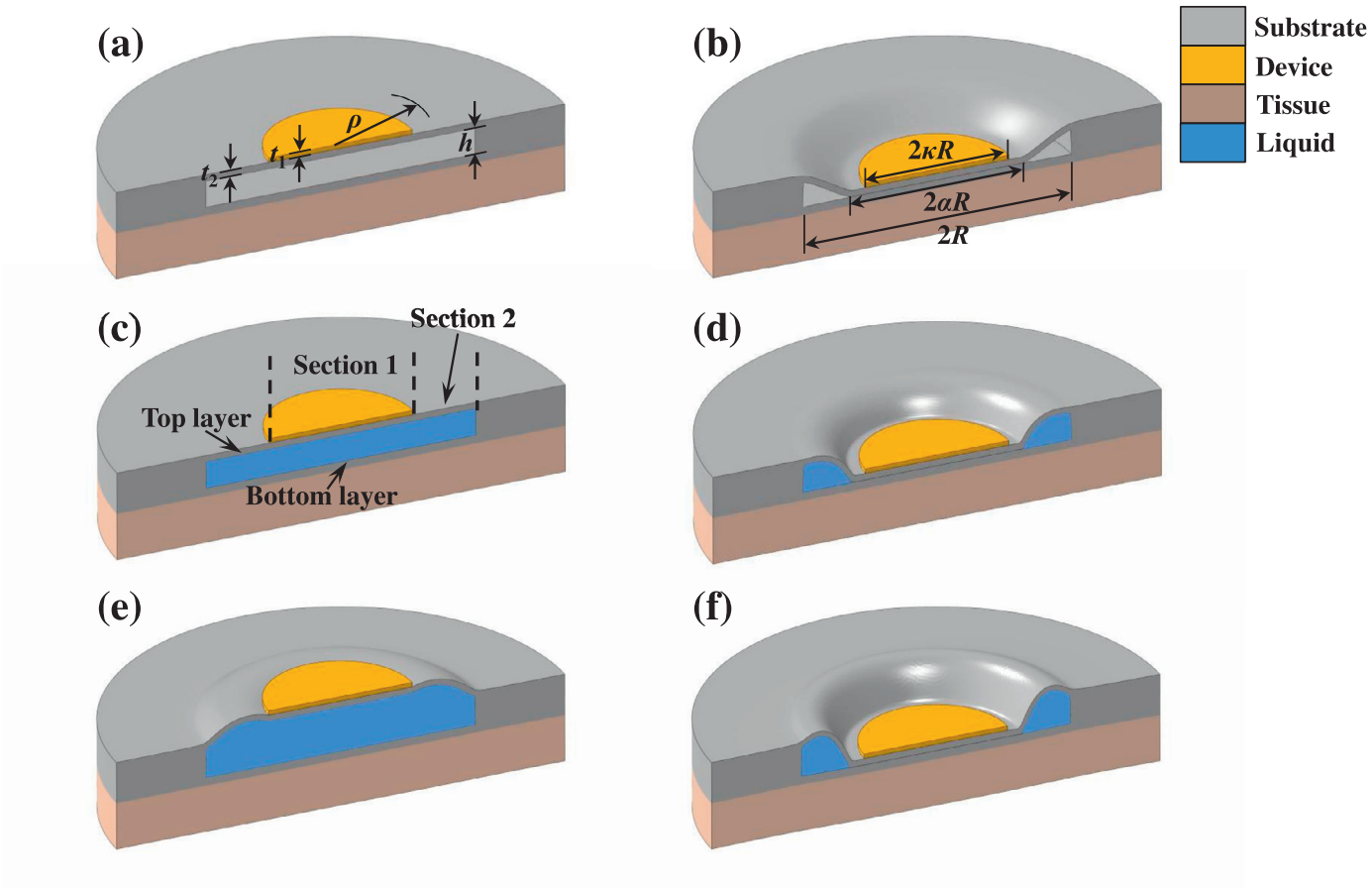

Fig. 1. Cross-sectional schematic illustrations of **(a, c, e)** the circular cavities and **(b, d, f)** their collapsed states **(a, b)** filled with air, **(c, d)** filled with liquid, and **(e, f)** overfilled by liquid.

(Ma et al., 2017). With the stress-free state (Fig. 1a and c) defined as the ground state (i.e., zero energy), the total potential energy due to roof collapse is (Huang et al., 2005)

$$U_{total} = U_{deformation} - \pi\alpha^2 R^2\gamma, \tag{1}$$

where $U_{deformation}$ is the deformation energy of the top layer and the device (and the deformation energy of the bottom layer is negligible (Ma et al., 2017)), and γ is the work of adhesion between the top and bottom surfaces of the cavity. The device and top layer are modeled as plates because their thicknesses are much less than their radius, $t_1 << R$ and $t_2 << R$. The normalized total potential energy in Eq. (1) then takes the form

$$\frac{R^2U_{total}}{Dh^2} = \frac{R^2U_{deformation}}{Dh^2} - \pi\gamma'\alpha^2, \tag{2}$$

where $\gamma' = \gamma R^4/Dh^2$ is the normalized work of adhesion.

2.1. Air-filled cavity

The deflection w is -h in the collapsed region ($0 \le \rho \le \alpha R$, where ρ is the polar coordinate, Fig. 1a). For an air-filled cavity, the deflection w in the uncollapsed region ($\alpha R < \rho \le R$) satisfies the equilibrium equation in polar coordinates (Blaauwendraad, 2010),

$$\left(\frac{d^2}{d\rho^2} + \frac{1}{\rho}\frac{d}{d\rho}\right)\left(\frac{d^2}{d\rho^2} + \frac{1}{\rho}\frac{d}{d\rho}\right)w = 0. \tag{3}$$

The boundary conditions are

$$w\big|_{\rho=\alpha R} = -h, \tag{4a}$$

$$\frac{dw}{d\rho}\Big|_{\rho=\alpha R} = 0, \tag{4b}$$

$$w\big|_{\rho=R} = 0, \tag{4c}$$

$$\frac{dw}{d\rho}\Big|_{\rho=R} = 0. \tag{4d}$$

The deformation energy in the collapsed region ($0 \le \rho \le \alpha R$) is zero because its deflection keeps a constant (w ==-h). Therefore, the deformation energy of the whole region ($0 \le \rho \le R$) is obtained from w by the plate theory as (Timoshenko and Woinowsky-Krieger, 1959)

$$U_{deformation} = \int_{\alpha R}^{R}\left\{D'_{11}\left[\left(\frac{\partial^2 w}{\partial\rho^2}\right)^2 + \left(\frac{1}{\rho}\frac{\partial w}{\partial\rho}\right)^2\right] + 2D'_{12}\frac{\partial^2 w}{\partial\rho^2}\left(\frac{1}{\rho}\frac{\partial w}{\partial\rho}\right)\right\}\rho\pi\,d\rho, \tag{5}$$

where D'_{11} and D'_{12} are the bending stiffness; $D'_{11} = D = E_2t_2^3/[12(1-\nu_2^2)]$ and $D'_{12} = \nu_2 D'_{11}$ ($\nu_2 = 0.5$) for Section 2 ($\kappa R < \rho \le R$) in Fig. 1c that does not have the device (i.e., top layer only), and $D'_{11} = mD$ and $D'_{12} = \eta mD$ for Section 1 ($0 \le \rho \le \kappa R$) in Fig. 1c consisting of both the top layer and the device, with m and η given in terms of the plane-strain moduli $\bar{E}_1 = E_1/(1-\nu_1^2)$ and $\bar{E}_2 = E_2/(1-\nu_2^2)$ as (Daniel et al., 1994) (See Appendix A

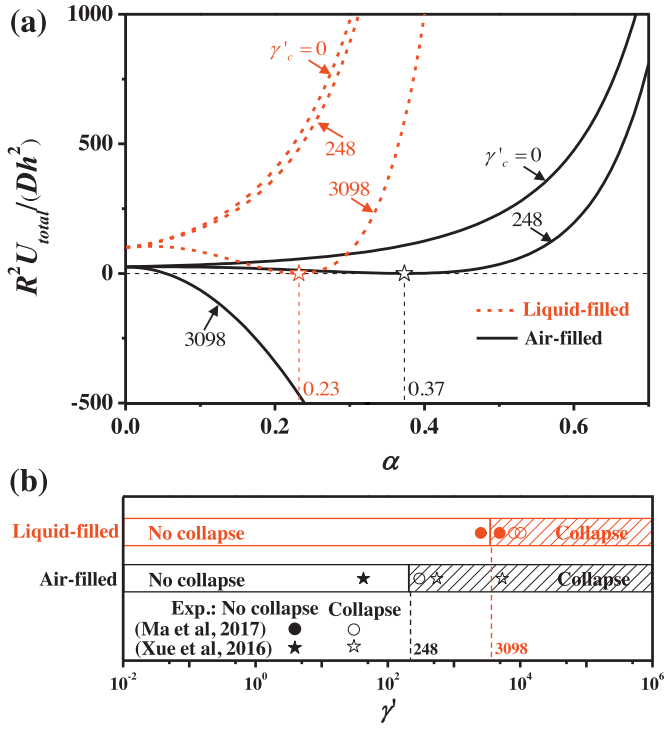

Fig. 2. (a) Normalized total potential energy $[R^2U_{total}/(Dh^2)]$ versus normalized collapse radius (α) when the device radius is less than the collapse radius ($\kappa < \alpha$) for several normalized works of adhesion (γ') for air- and liquid-filled cavities. **(b)** Comparison between collapse model (non-shaded and shaded regions for no collapse and collapse) and experimental results (solid and hollow symbols for no collapse and collapse). (For interpretation of the references to color in this figure legend, the reader is referred to the web version of this article.)

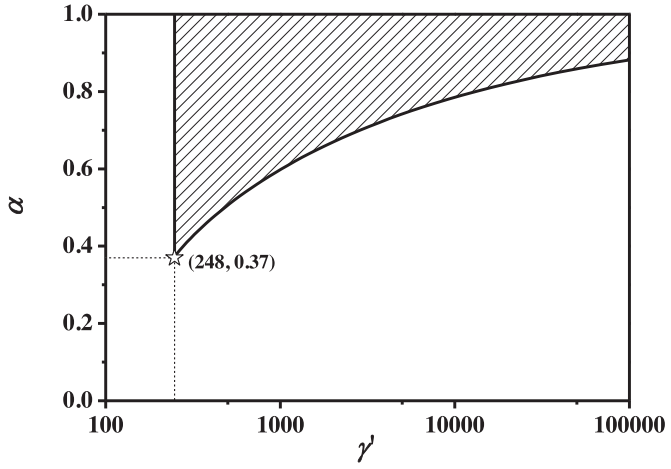

Fig. 3. Normalized collapse radius (α) versus normalized work of adhesion (γ') when the device radius is less than the collapse radius ($\kappa < \alpha$).

for details)

$$m = \frac{\left(t_1^2\bar{E}_1 - t_2^2\bar{E}_2\right)^2 + 4t_1t_2(t_1+t_2)^2\bar{E}_1\bar{E}_2}{t_2^3\bar{E}_2(t_1\bar{E}_1 + t_2\bar{E}_2)}, \tag{6a}$$

$$\eta = \frac{\left(t_1^3\bar{E}_1\nu_1 + t_2^3\bar{E}_2\nu_2\right)\left(t_1\bar{E}_1 + t_2\bar{E}_2\right)^2 + 3t_1t_2(t_1+t_2)^2\bar{E}_1\bar{E}_2\left(t_1\bar{E}_1\nu_2 + t_2\bar{E}_2\nu_1\right)}{(t_1\bar{E}_1 + t_2\bar{E}_2)\left(t_1^2\bar{E}_1 - t_2^2\bar{E}_2\right)^2 + 4t_1t_2(t_1+t_2)^2\bar{E}_1\bar{E}_2}. \tag{6b}$$

Two separate scenarios are considered.

(i) The collapse radius is larger than the device radius ($\alpha > \kappa$). In the uncollapsed region the solution of Eqs. (3) and (4) is

$$w = -h\frac{(1-\alpha^2)\left(1-\frac{\rho^2}{R^2}\right) + 2\frac{\rho^2}{R^2}\ln\frac{\rho}{R} + 2\alpha^2\left[\frac{\rho^2}{R^2}\ln\frac{\alpha R}{\rho} - \left(1+2\ln\frac{\rho}{R}\right)\ln\alpha\right]}{(1-\alpha^2)^2 - 4\alpha^2(\ln\alpha)^2}. \tag{7}$$

Its substitution into Eq. (5) gives the deformation energy

$$U_{deformation} = \frac{Dh^2}{R^2}\frac{8\pi(1-\alpha^2)}{(1-\alpha^2)^2 - 4\alpha^2(\ln\alpha)^2}. \tag{8}$$

Here the elastic properties and thickness of the device do not appear because the device remains flat over the collapsed region, i.e., it does not deform. Therefore the normalized total potential energy in Eq. (2) depends only on α, and is shown by the solid black lines in Fig. 2 for three normalized work of adhesion $\gamma' = 0$, 248 and 3098. These three curves converge to $R^2U_{total}/(Dh^2) = 8\pi$ at $\alpha = 0$, which represents the collapse state with a single point contact between top and bottom layers. The curve for $\gamma' = 0$ increases monotonically, which suggests no collapse if there is no adhesion. As γ' increases, the curve (e.g., for $\gamma' = 248$) displays a local minimum, which corresponds to roof collapse, and the collapse radius is αR at this minimum. For $\gamma' < 248$, the minimum total potential energy is positive, which is larger than zero for the ground state of no collapse and no deformation such that roof collapse is not stable, and will spring back to the uncollapsed state upon disturbance. Zero minimum total potential energy for $\gamma' = 248$, together with the monotonicity of minimum total potential energy with γ' from Eq. 2, shows that for $\gamma' < 248$, the minimum total potential energy is positive, which is larger than zero for the ground state of no collapse and no deformation such that roof collapse is not stable, and will spring back to the uncollapsed state upon disturbance. Only for $\gamma' > 248$ the minimum total potential energy is negative, and roof collapse becomes stable. The critical normalized work of adhesion governing the collapse is $\gamma'_c = 248$. This critical normalized work of adhesion is obtained using the plate theory, which requires $t_2 << R$. The experimental results (Xue et al., 2017; Ma et al., 2017) satisfying $R/t_2 \geq 10$ are compared with the collapse model [Xue et al.'s (2017) experiments had the same thickness for the top and bottom layers. Therefore its work of adhesion is scaled by 0.5 in order to compare with the collapse model for a single (top) layer]. Fig. 2b gives the normalized work of adhesion with several R, t_2 and h for air-filled cavity in PDMS or Ecoflex (work of adhesion: $\sim 40\ mJ/m^2$) determined from the literatures (Xue et al., 2017; Ma et al., 2017), which agrees well with $\gamma'_c = 248$. Fig. 3 shows the collapse radius versus the normalized work of adhesion γ'. It starts from the point ($\gamma' = 248$, $\alpha = 0.37$) and increases with γ'. The requirement of the collapse radius being larger than the device radius ($\alpha > \kappa$) for this section means that κ should be lower than the curve in Fig. 3 for $\gamma' > \gamma'_c = 248$, or any κ (<1) for $\gamma' < \gamma'_c = 248$, as denoted by the non-shaded region in Fig. 3.

(ii) The collapse radius is smaller than the device radius ($\alpha < \kappa$). For the device radius larger than the critical radius of collapse in Fig. 3, roof collapse depends on the device elastic properties and thickness because the device is bent in the uncollapsed region. The continuity conditions across the junction between Sections 1 and 2 are

$$[w]\big|_{\rho=\kappa R} = 0, \tag{9a}$$

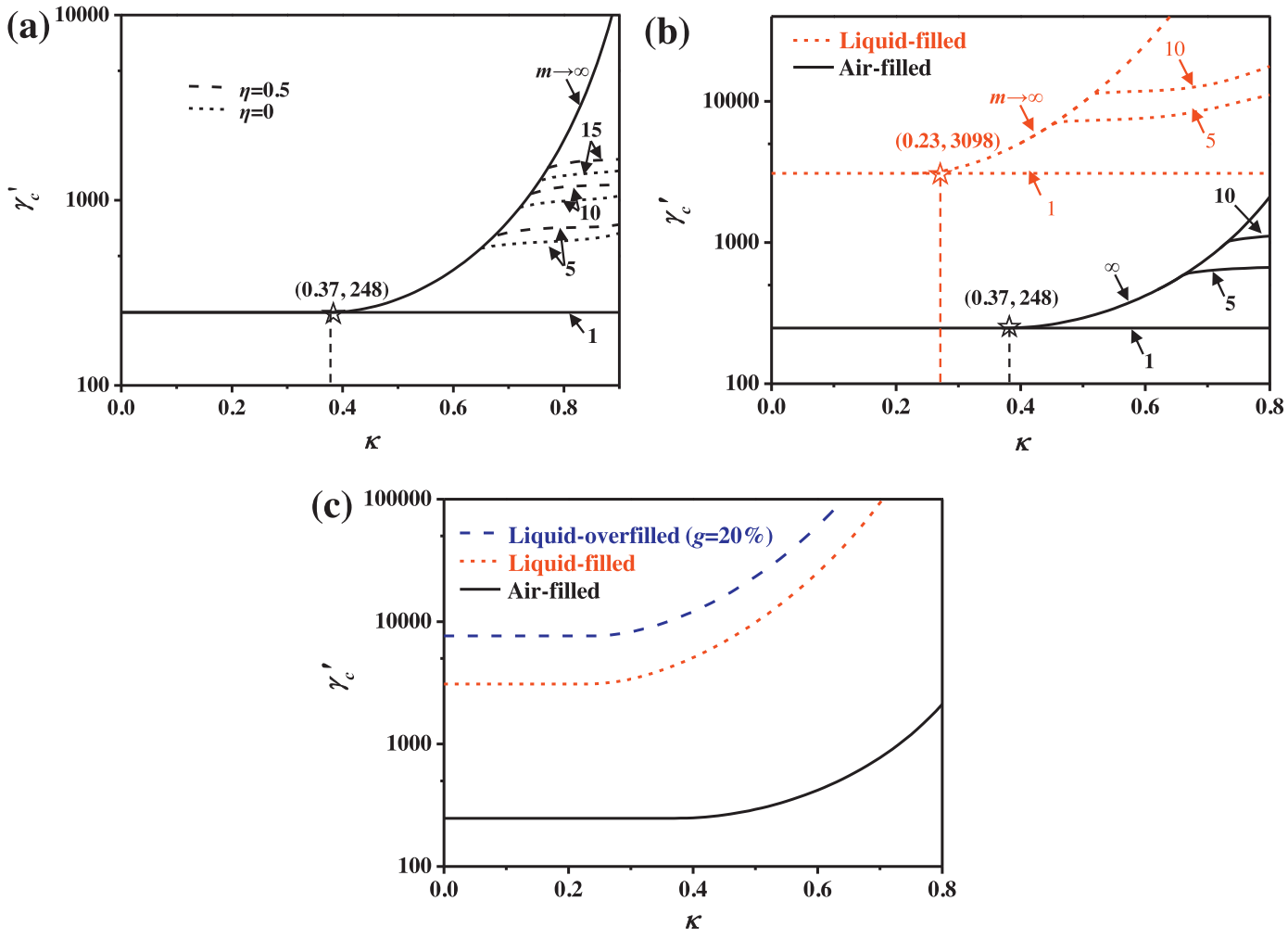

Fig. 4. Critical normalized work of adhesion (γ'_c) versus normalized device radius (κ) for **(a)** air-filled cavities (with $m=\infty$, 15, 10, 5 and 1 and $\eta=0$ and 0.5), **(b)** air- and liquid-filled cavities (with $m=\infty$, 10, 5 and 1 and $\eta=0.5$), and **(c)** air-, liquid-filled and liquid-overfilled cavities ($m=\infty$).

$$\left[\frac{dw}{d\rho}\right]\Big|_{\rho=\kappa R}=0, \tag{9b}$$

$$[m_{\rho\rho}]\big|_{\rho=\kappa R}=0, \tag{9c}$$

$$[S]\big|_{\rho=\kappa R}=0, \tag{9d}$$

where $[u]=u^+-u^-$ represents the jump of u, $m_{\rho\rho}=-D'_{11}(d^2w/d\rho^2)-(D'_{12}/\rho)(dw/d\rho)$ and $S=-D'_{11}[(d^3w/d\rho^3)+(1/\rho)(d^2w/d\rho^2)-(1/\rho^2)(dw/d\rho)]$ are the moment and shear force, respectively. Substitution of w obtained from Eqs. (3), (4) and (9) into Eq. (5) gives the deformation energy. Minimization of the total potential energy in Eq. (2) with respect to α determines the collapsed state. The critical normalized work of adhesion γ'_c is then obtained by setting the minimum total potential energy to be zero, and it depends on m, η and κ, i.e., $\gamma'_c=f(m,\eta,\kappa)$. Fig. 4a shows γ'_c versus κ for $\eta=0$ and 0.5 and several values of m, where $m=1$ represents the top layer only (i.e., no device).

The limit $m\to\infty$ corresponds to a rigid device, for which η disappears in the analysis, i.e., $\gamma'_c=f(\kappa)$. For $\kappa<0.37$ (i.e., the smallest normalized collapse radius in Fig. 3), the device is never bent, therefore $\gamma'_c=248$. For $\kappa>0.37$, it is shown in Appendix B that, at the critical state corresponding to γ'_c, the collapse radius is the identical to the device radius, i.e., $\alpha=\kappa$. Its substitution into Eq. (8) gives the deformation energy $U_{deformation}=\frac{Dh^2}{R^2}\frac{8\pi(1-\kappa^2)}{(1-\kappa^2)^2-4\kappa^2(\ln\kappa)^2}$ at the critical state corresponding to γ'_c. The critical normalized work of adhesion γ'_c is then obtained by setting the minimum total potential energy to be zero as

$$\gamma'_c=f(\kappa)=\begin{cases}248\ (\kappa<0.37)\\ \dfrac{8(1-\kappa^2)}{\kappa^2[(1-\kappa^2)^2-4\kappa^2(\ln\kappa)^2]}\ (\kappa>0.37),\end{cases} \tag{10}$$

which is also shown in Fig. 4a. It should be pointed out that, for all practical applications, the simple equation above is accurate because all curves with finite m merge into the one for the rigid device ($m\to\infty$) in Fig. 4a. For example, for a 100-μm-thick silicon device ($E_1=130$ GPa and $\nu_1=0.27$) with a normalized radius $\kappa=2/3$, Eq. (10) is accurate if the top layer is thinner than 15 mm for Ecoflex ($E_2=60$ kPa and $\nu_2=0.5$), or 6 mm for PDMS ($E_2=1$ MPa and $\nu_2=0.5$). For a 100 nm-thick silicon device with $\kappa=2/3$, these upper limits scale down proportionally to 15 μm for Ecoflex and 6 μm for PDMS.

2.2. Liquid-filled cavity

A cavity filled with liquid helps to prevent collapse (Ma et al., 2017). For a liquid-filled cavity, the boundary condition (4) and continuity condition (9) still hold, but the equilibrium Eq. (3)

becomes

$$\left(\frac{d^2}{d\rho^2}+\frac{1}{\rho}\frac{d}{d\rho}\right)\left(\frac{d^2}{d\rho^2}+\frac{1}{\rho}\frac{d}{d\rho}\right)w=p, \tag{11}$$

where p is the liquid pressure to be determined from the conservation of the cavity volume because the bulk modulus of liquid (e.g., ~2 GPa for water) is much larger than the elastic modulus of substrate [e.g., PDMS (20 kPa ~ 3 MPa, Xue et al., 2017) and Ecoflex (60 kPa, Ma et al., 2017)] surrounding the liquid such that the liquid can be considered as incompressibe),

$$\int_0^R w\cdot 2\rho\pi\cdot \mathrm{d}\rho=0. \tag{12}$$

The dashed red curve in Fig. 2 shows the normalized total potential energy for the system with the liquid-filled cavity. For the normalized works of adhesion $\gamma'=0$, 248 and 3098, all curves for the liquid-filled cavity are much higher than those for the air-filled cavity. Here 3098 is the critical normalized work of adhesion for the liquid-filled cavity and small device radius (such that the device does not bend), and it is much larger than the corresponding 248 for the air-filled cavity. Fig. 2b gives the normalized work of adhesion with several R, t_2 and h for liquid-filled cavity in Ecoflex (work of adhesion: 16.8 mJ/m^2) determined from the literature (Ma et al., 2017). These experimental results in the literature agree reasonably well with our collapse model. The slight discrepancies between theoretical and experimental results for liquid-filled cavity may result from that the work of adhesion estimated by contact angle formula may differ from the actual values of the materials used in the experiments. For all values of m (that may involve device bending) and $\eta=0.5$, the curves of γ'_c for the liquid-filled cavity in Fig. 4b are much higher than the air-filled cavity. All of these calculations suggest that the liquid-filled cavity is less susceptible to collapse.

The limit of a rigid device ($m\to\infty$), which is still a good approximation for all applications involving the liquid-filled cavity, has the critical normalized work of adhesion

$$\gamma'_c=\begin{cases}3098\ (\kappa<0.23)\\ \dfrac{32(1-\kappa^2)^3}{\kappa^2[(1-\kappa^2)^2(\kappa^4-14\kappa^2+1)-24\kappa^2(1-\kappa^4)\ln\kappa-16\kappa^2(\kappa^4+\kappa^2+1)(\ln\kappa)^2]}\ (\kappa>0.23),\end{cases} \tag{13}$$

which is much larger than Eq. (10) for the air-filled cavity, as shown in Fig. 4b.

2.3. Liquid-overfilled cavity

A cavity overfilled with liquid further helps to prevent collapse. Here the overfill is represented by the percentage of liquid overfill $g=V_{liquid}/V_{cavity}-1$, where V_{liquid} is the volume of the injected liquid, and $V_{cavity}=\pi R^2h$ is the cavity volume. The boundary condition (4), continuity condition (9) and equilibrium Eq. (11) still hold, but Eq. (12) from liquid incompressibility now becomes

$$\int_0^R w\cdot 2\rho\pi\cdot \mathrm{d}\rho=\pi R^2hg. \tag{14}$$

The ground state (before collapse) has non-zero energy now because the overfill of the liquid induces deformation in the top layer (and possibly the device). A detailed analysis of collapse is given in Appendix C. The limit of a rigid device ($m\to\infty$) is still a good approximation for all practical applications, and has the critical normalized work of adhesion

$$\gamma'_c=\begin{cases}3098+20876g\ (\kappa<0.23)\\ \dfrac{32\{(1-\kappa^2)^2[(1-\kappa^2)^2+12g^2+6g(1+\kappa^2)]+24g\kappa^2(1-\kappa^2)\ln\kappa-48g^2\kappa^2(\ln\kappa)^2\}}{\kappa^2(1-\kappa^2)[(1-\kappa^2)^2(\kappa^4-14\kappa^2+1)-24\kappa^2(1-\kappa^4)\ln\kappa-16\kappa^2(\kappa^4+\kappa^2+1)(\ln\kappa)^2]}-\dfrac{96g^2}{\kappa^2}\ (\kappa>0.23),\end{cases} \tag{15}$$

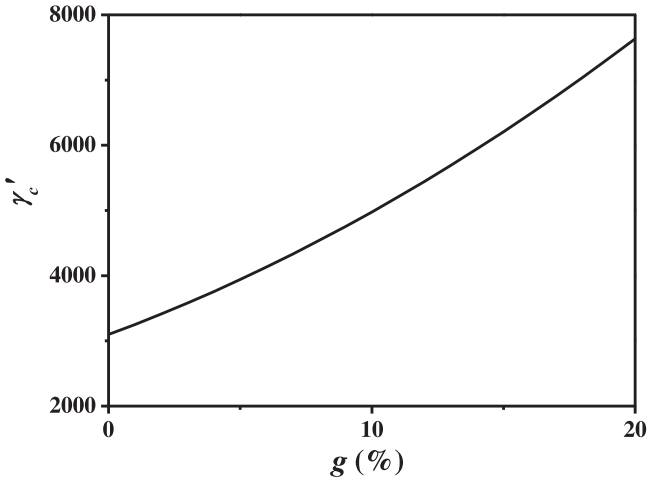

Fig. 5. Critical normalized work of adhesion (γ'_c) versus liquid overfill percentage (g) when the device radius is less than the collapse radius ($\kappa<\alpha$).

where γ'_c ==3098+20876g for $\kappa<0.23$ is a linear fit of the critical normalized work of adhesion (γ'_c) versus the liquid-overfill percentage (g) for $\alpha>\kappa$ shown in Fig. 5. Fig. 4c shows the critical normalized work of adhesion for a 20% liquid-overfilled cavity is much larger than those for the air- and liquid-filled cavities. While liquid overfill is more effective to prevent roof collapse, it should be cautioned that a large overfill may lead to significant bending of the device.

3. Concluding remarks

Axisymmetric models of roof collapse are established in this paper to give the critical adhesion for liquid-overfilled, liquid- and air-filled cavities. Scaling laws are established for the critical normalized work of adhesion via the normalized bending stiffness (m) and normalized device radius (κ). The liquid-overfilled cavity gives the largest critical work of adhesion, and is therefore most effective to prevent roof collapse.

Acknowledgments

X.W., Y.M. and X.F. acknowledge the support from the National Basic Research Program of China (Grant No. 2015CB351900), National Natural Science Foundation of China (Grant Nos. 11202178, 11402135, 11320101001) and Natural Science Foundation of Hunan Province (Grant No. 14JJ3082). Y.H. acknowledges the support from NSF (Grant Nos. DMR1121262, CMMI1300846, CMMI1400169 and CMMI1534120) and the NIH (Grant No. R01EB019337). Y.X. gratefully acknowledges support from the Ryan Fellowship and the Northwestern University International Institute for Nanotechnology.

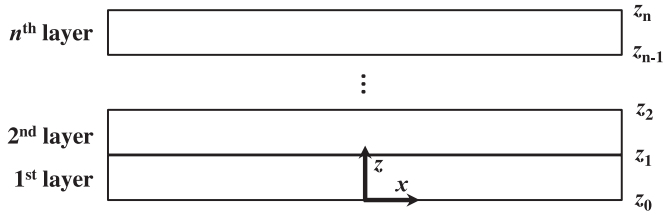

Fig. A1. Isotropic n-layers laminate with coordinate notation.

Appendix A

Daniel et al. (1994) gave the bending stiffness of the isotropic n-layers laminate as

$$D'_{11} = \frac{1}{3}\sum_{k=1}^{n}\left\{\frac{E_k}{1-\nu_k^2}\left[(z_k - h_{neutral})^3 - (z_{k-1} - h_{neutral})^3\right]\right\}, \quad \text{(A1a)}$$

$$D'_{12} = \frac{1}{3}\sum_{k=1}^{n}\left\{\frac{\nu_k E_k}{1-\nu_k^2}\left[(z_k - h_{neutral})^3 - (z_{k-1} - h_{neutral})^3\right]\right\}, \quad \text{(A1b)}$$

where E_k and ν_k are the modulus and Poisson's ratio of the kth layer, z_k and z_{k-1} are the z-coordinates of the upper and lower surfaces of the kth layer as Fig. A1. $h_{neutral}$ is the distance from the bottom to the neutral mechanical plane and is given by

$$h_{neutral} = \frac{\sum_{k=1}^{n} E_k\left(z_k^2 - z_{k-1}^2\right)}{2\sum_{k=1}^{n} E_k(z_k - z_{k-1})}. \quad \text{(A2)}$$

The bilayer structure consists of the device (thickness t_1, modulus E_1, and Poisson's ratio ν_1) and top layer (thickness t_2, modulus E_2, and Poisson's ratio ν_2), together with Eqs. (A1) and (A2) gives m and η as Eq. (6).

Appendix B

A rigid device ($m \to \infty$) cannot deform, and therefore the collapse radius must be at least the device radius, i.e., $\alpha > \kappa$. Eqs. (1) and (8) give the derivative of the total potential energy as

$$\frac{R^2}{Dh^2}\frac{\partial U_{total}}{\partial \alpha} = \frac{16\pi\alpha(\alpha^2 - 2\ln\alpha - 1)^2}{\left[(1-\alpha^2)^2 - 4\alpha^2(\ln\alpha)^2\right]^2} - 2\pi\gamma'\alpha. \quad \text{(B1)}$$

For all the shaded region in Fig. 3, $\partial U_{total}/\partial\alpha \geq 0$, which indicates that the total potential energy decreases with α such that its minimum total potential energy occurs at $\alpha = \kappa$, i.e., the collapse radius is the identical to the device radius.

Appendix C

The deflection due to liquid overfill, prior to roof collapse, satisfies the same equilibrium Eq. (11), continuity conditions in Eq. (9), liquid incompressibility in Eq. (14), with the boundary conditions

$$\frac{dw}{d\rho}\Big|_{\rho=0} = 0, \quad \text{(C1a)}$$

$$S\Big|_{\rho=0} = 0, \quad \text{(C1b)}$$

$$w\Big|_{\rho=R} = 0, \quad \text{(C1c)}$$

$$\frac{dw}{d\rho}\Big|_{\rho=R} = 0. \quad \text{(C1d)}$$

Substitution of its solution in Eq. (5), with the lower limit of integration changed to 0, gives the deformation energy before collapse, $U_{initial}$. For $\alpha > \kappa$, it yields a simple expression $U_{initial} = 96\pi g^2 Dh^2/R^2$. Roof collapse occurs when the minimal total potential energy is less than $U_{initial}$.

References

Blaauwendraad, J., 2010. Plates and FEM. Springer.

Chen, Y., Lu, B., Chen, Y., Feng, X., 2016. Biocompatible and ultra-flexible inorganic strain sensors attached to skin for long-term vital signs monitoring. IEEE Electron Device Lett. 37, 496–499.

Cheng, H., Wu, J., Li, M., Kim, D.H., Kim, Y.S., Huang, Y., Kang, Z., Hwang, K.C., Rogers, J.A., 2011. An analytical model of strain isolation for stretchable and flexible electronics. Appl. Phys. Lett. 98, 06.

Chortos, A., Liu, J., Bao, Z., 2016. Pursuing prosthetic electronic skin. Nat. Mater. 15, 937–950.

Daniel, I.M., Ishai, O., Daniel, I.M., Daniel, I., 1994. Engineering Mechanics of Composite Materials. Oxford university press New York.

De Boer, M., Michalske, T., 1999. Accurate method for determining adhesion of cantilever beams. J.Appl. Phys. 86, 817–827.

Huang, Y.Y., Zhou, W., Hsia, K.J., Menard, E., Park, J.U., Rogers, J.A., Alleyne, A.G., 2005. Stamp Collapse in Soft Lithography. Langmuir 21, 8058–8068.

Koh, A., Kang, D., Xue, Y., Lee, S., Pielak, R.M., Kim, J., Hwang, T., Min, S., Banks, A., Bastien, P., Manco, M.C., Wang, L., Ammann, K.I., Jang, K.I., Won, P., Han, S., Ghaffari, R., Paik, U., Slepian, M.J., Balooch, G., Huang, Y., Rogers, J.A., 2016. A soft, wearable microfluidic device for the capture, storage, and colorimetric sensing of sweat. Sci. Transl. Med. 8, 366ra165.

Kim, D.H., Kim, Y.S., Wu, J., Liu, Z., Song, J., Kim, H.S., Huang, Y.Y., Hwang, K.C., Rogers, J.A., 2009. Ultrathin silicon circuits with strain-isolation layers and mesh layouts for high-performance electronics on fabric, vinyl, leather, and paper. Adv. Mater. 21, 3703–3707.

Lee, C.H., Ma, Y., Jang, K.I., Banks, A., Pan, T., Feng, X., Kim, J.S., Kang, D., Raj, M.S., McGrane, B.L., 2015. Soft core/shell packages for stretchable electronics. Adv. Funct. Mater. 25, 3698–3704.

Ma, Y.J., Pharr, M., Wang, L., Kim, J., Liu, Y., Xue, Y.G., Ning, R., Wang, X.F., Chung, H., Feng, X., Rogers, J.A., Huang, Y.G., 2017. Soft elastomers with ionic liquid–filled cavities as strain isolating substrates for wearable electronics. Small 13, 1602954.

Mastrangelo, C.H., Hsu, C., 1993. Mechanical stability and adhesion of microstructures under capillary forces. I. Basic theory. J. Microelectromech. Sys. 2, 33–43.

Robinson, A., Aziz, A., Liu, Q., Suo, Z., Lacour, S., 2014. Hybrid stretchable circuits on silicone substrate. J. Appl. Phys. 115, 143511.

Romeo, A., Liu, Q., Suo, Z., Lacour, S.P., 2013. Elastomeric substrates with embedded stiff platforms for stretchable electronics. Appl. Phys. Lett. 102, 13.

Timoshenko, S.P., Woinowsky-Krieger, S., 1959. Theory of Plates and Shells. McGraw-hill.

Webb, R.C., Ma, Y., Krishnan, S., Li, Y., Yoon, S., Guo, X., Feng, X., Shi, Y., Seidel, M., Cho, N.H., 2015. Epidermal devices for noninvasive, precise, and continuous mapping of macrovascular and microvascular blood flow. Sci. Adv. 1, e1500701.

Wu, J., Li, M., Chen, W.Q., Kim, D.H., Kim, Y.-S., Huang, Y.G., Hwang, K.C., Kang, Z., Rogers, J.A., 2010. A strain-isolation design for stretchable electronics. Acta Mech. Sinica 26, 881–888.

Xu, F., Zhu, Y., 2012. Highly conductive and stretchable silver nanowire conductors. Adv. Mater. 24, 5117–5122.

Xue, Y., Kang, D., Ma, Y., Feng, X., Rogers, J.A., Huang, Y., 2017. Collapse of microfluidic channels/reservoirs in thin, soft epidermal devices. Extreme Mech. Lett. 11, 18–23.